Flutter Phenomenon and Safety Implications in Transonic Flow

Zihan Feng

Leicester Institute, Dalian University of Technology, Panjin, 124000, China

fengzihan@mail.dlut.edu.cn

Abstract. As advancements in aircraft manufacturing technology persistently elevate the boundaries of flight speed, challenges emerge when aircraft velocities verge on sonic speeds. Notably, empirical observations have highlighted instances of pronounced vibrations and, in extreme cases, structural failures, casting shadows over flight stability and safety. This research endeavors to dissect the ramifications of shock waves and flutter phenomena, precipitated by fluid discontinuities during supersonic flight, on the overarching safety of aircraft. Methodologically, the study delineates a series of simulation protocols, commencing with the derivation of simplified functions representing the aircraft's 2D contour, followed by error function computations, and finally, using the finite difference method in conjunction with the successive over-relaxation (SOR) iterative technique to model the aircraft's velocity distribution. Preliminary findings indicate that for β values spanning 0.1, 0.15, and 0.175, the surrounding airflow retains its continuity and stability, with the Mach number's rate of change exhibiting a decelerating trend. Conversely, at a β threshold of 0.2, the airflow descends into turbulence, manifesting in erratic Mach number fluctuations. Such fluidic discontinuities underscore potential threats to the aircraft's flight safety, necessitating further exploration and mitigation strategies.

Keywords: Flutter, successive over-relaxation, transonic flight.

1. Introduction

In supersonic flow conditions, the aircraft's aerodynamic performance is often greatly affected due to the interaction of the shock boundary layer on its upper surface and airflow separation, causing flow instability. Additionally, turbulence frequently occurs as the aircraft's Mach number or angle of attack rises, resulting in sustained oscillations during supersonic flight. These oscillations, along with the associated loads, can lead to structural fatigue and flight accidents [1].

Common wing airfoil types include symmetrical, cambered, double-cambered, and variable-camber airfoil. A symmetrical airfoil has the same curvature on both upper and lower surfaces, performing well at low speeds and zero angle of attack but generating higher drag at high speeds and large angles [2]. A cambered airfoil has a greater curvature on the upper surface than the lower surface, suitable for higher-speed flight and moderate angles of attack, providing higher lift and lower drag [3]. A double-cambered airfoil has a curvature on both upper and lower surfaces, suitable for higher-speed flight and large angles of attack, offering higher lift and lower drag [4]. A variable-camber airfoil, such as a supercritical airfoil, is designed with a thicker profile closer to the leading edge and a thinner profile towards the trailing edge, reducing shock wave drag and enhancing supersonic flight performance [5].

The requirements for modern aircraft design extend beyond higher speed and stability, encompassing various other aspects. The growing environmental protection awareness necessitates aircraft designs that address noise reduction, emissions reduction, improved fuel efficiency, and lower carbon footprint. Additionally, the increasing expectations for passenger comfort drive the need for aircraft designers to provide a superior passenger experience while meeting flight performance requirements. Simulation of forces plays a crucial role in aircraft design, enabling us to understand the effects of forces on aircraft under different flight conditions, predict and optimize aircraft performance, and address challenges and issues encountered during specific flight states. The aerodynamic characteristics, structural strength, and control system response of aircraft can be evaluated using the results obtained from the force simulation, facilitating design optimization and

enhancing flight efficiency and safety. Therefore, force simulation research holds significant importance in the development of modern aircraft design [6].

2. Mechanism of Flutter during Transonic Process

Flutter is an aeroelastic phenomenon controlled by unstable aerodynamic forces. When an aircraft or structure is subjected to energy input or external disturbances, it exhibits a certain response speed. New excitation is produced when alternating momentum is generated within the system and fed back to the system. As a result, the system responds in the opposite direction to the original response speed, forming alternating velocities. Under the influence of the alternating action forces caused by the alternating velocities, the system may experience self-excited vibration, known as flutter. Flutter is an unstable vibration state that can negatively affect the safety of aircraft or structures. Therefore, it is necessary to consider and control flutter phenomena for aircraft and structural design to ensure system stability and safety [7].

During subsonic flight, weak disturbances in the gas propagate at the local speed of sound. However, due to the relatively slow flight speed of the aircraft, the disturbance propagation speed is faster than the aircraft speed, making it difficult for the disturbances to concentrate. Therefore, the distribution of flow parameters in the flow field is continuous. However, during supersonic flight, the aircraft's speed is faster than the disturbance propagation speed, causing the disturbances to concentrate and leading to discontinuities in the fluid. This results in concentrated and continuously amplified disturbances, which can significantly impact the safety of the aircraft.

3. Design Simulation Steps

3.1. Boundary Condition

Due to the different shapes of the wing positions, appropriate boundary conditions can be determined based on the x range to ensure that the velocity distribution satisfies physical laws and experimental observations.

When $x \in [1, 2]$, the range where the wing is located, the partial derivative of the fluid velocity with respect to x can be approximated as $U_\infty \cdot f'(x)$.

$$-\partial\varphi/\partial x = (U_\infty + u)\cdot f'(x) \approx U_\infty \cdot f'(x) \tag{1}$$

Where U_∞ is the free stream velocity far away from the object, u is the velocity component on the object surface, and $f'(x)$ is a function that describes the variation of velocity distribution with distance from the object surface.

The assumption that f(x) represents the wing shape and is given by $\beta\cdot\sin(\pi\cdot(x-1))$, where β is a constant, is based on a physical understanding of fluid flow and experimental observations. This assumption is commonly used in aerodynamics to model the shape of wings and other airfoils. The sine function is often used to approximate the wing's curvature, as it can capture the smooth and periodic variations in the wing shape. The constant β allows for scaling and adjusting the amplitude of the wing shape. This assumption has been validated through experimental testing and analysis, showing that the sinusoidal wing shape accurately represents the flow characteristics and performance of wings in various conditions [8].

By differentiating f(x), $f'(x)$ can be obtained as

$$f'(x) = \beta\cdot\pi\cdot\cos(\pi\cdot(x-1)) \tag{2}$$

This derivative describes the rate of change of the velocity distribution. Therefore, the boundary condition can be set as $\beta\cdot\pi\cdot\cos(\pi\cdot(x-1))$ to ensure that the velocity satisfies specific conditions at the object's surface.

Next, when x is in the range [0, 3] but not within the range [1, 2], the velocity distribution is constant, i.e., f(x) is a constant and equal to 0. According to the definition of boundary conditions, the boundary condition can be set as 0 to ensure that the velocity outside the object's surface is zero.

3.2. Finite Difference Method

The small disturbance equation (SDE) method uses central differencing to convert the original continuous derivative form into a discrete form, which can be used for normal loop calculations in Python code [9].

For the second derivative, the basic form of central differencing is as follows:

$$f''(x) = \frac{f(x+h) - 2f(x) + f(x-h)}{h^2} + O(h) \tag{3}$$

Assuming

$$K = 1 - M^2 = 1 - M_\infty^2 - (\gamma + 1) \cdot M_\infty^2 \cdot \frac{\varphi_{i+1,j} - \varphi_{i-1,j}}{2\Delta h} \tag{4}$$

Based on Fig. 1, the SDE can be written as

$$K_{i-1,j}(\varphi_{i,j} - 2\varphi_{i-1,j} + \varphi_{i-2,j}) + (\varphi_{i,j+1} - 2\varphi_{i,j} + \varphi_{i,j-1}) = 0 \tag{5}$$

Based on Fig. 2, the SDE can be written as

$$K_{i,j}(\varphi_{i+1,j} - 2\varphi_{i,j} + \varphi_{i-1,j}) + (\varphi_{i,j+1} - 2\varphi_{i,j} + \varphi_{i,j-1}) = 0 \tag{6}$$

Combining equations (3-5) and (3-6), the equation can be written as

$$\frac{\mu K_{i-1,j}(\varphi_{i-2,j} - 2\varphi_{i-1,j}) + (\varphi_{i,j+1} + \varphi_{i,j-1}) + (1-\mu)K_{i,j}(\varphi_{i+1,j} + \varphi_{i-1,j})}{(2 + 2(1-\mu)K_{i,j} - \mu K_{i-1,j}} - \varphi_{i,j} = 0 \tag{7}$$

Where, μ=0 for M<1; μ=1 for M≥ 1.

At the same time, there may be $\varphi_{i,j-1}$ outside the range under boundary conditions. In this case, the central differencing method, $f'(x) \approx \frac{f(x+h) - f(x-h)}{2h}$, can also be used to represent $\varphi_{i,j-1}$ by the point $\varphi_{i,j+1}$ within the boundary range:

$$\varphi_{i,j-1} = \varphi_{i,j+1} - 2 \cdot h \cdot U_{-}\infty \cdot f'(x) \tag{8}$$

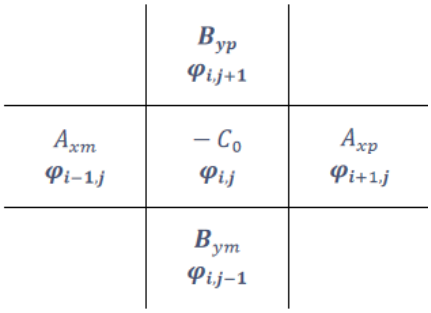

Figure 1. The difference scheme when M<1 (Photo/Picture credit: Original)

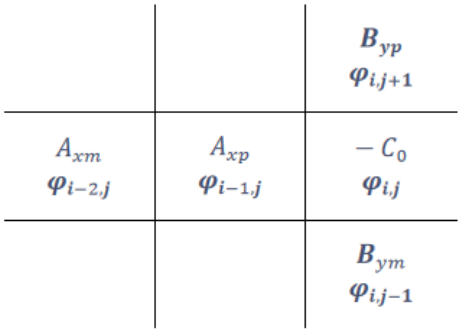

Figure 1. The difference scheme when M>1 (Photo/Picture credit: Original)

3.3. Error Function

Since the central differencing method introduces differences between the approximate and true values, an error function is needed to evaluate the accuracy of the calculated results. Therefore, by iterating through the elements of the array and calculating the approximate solution of the difference equation based on the values of adjacent elements, the difference between the approximate solution and the true solution is calculated and accumulated in the error. Finally, the average value of the error is returned as the result. An error function is designed accordingly, and in the main function, iteration is required until the error is less than e-7 before the true result can be output.

The error can be obtained using the following formula:

$$O(h) = \frac{\mu \cdot K_{i-1,j}(\varphi_{i-2,j} - 2\varphi_{i-1,j}) + (\varphi_{i,j+1} + \varphi_{i,j-1}) + (1-\mu)K_{i,j}(\varphi_{i+1,j} + \varphi_{i-1,j})}{(2 + 2(1-\mu)K_{i,j} - \mu K_{i-1,j}} - \varphi_{i,j} \tag{9}$$

3.4. SOR Method

In the SOR function, the SOR iteration method updates the solution vector step by step based on the discretized partial differential equation until the convergence condition is met.

First, the SOR factor is set to a relaxation factor with a value of 1.0 [10]. The function uses two nested loops to iterate through the inner grid points of Newphi (excluding the boundary points) and calculates the residual at the current point (i, j) as

$$d\varphi = \frac{\mu K_{i-1,j}(\varphi_{i-2,j} - 2\varphi_{i-1,j}) + (\varphi_{i,j+1} + \varphi_{i,j-1}) + (1-\mu)K_{i,j}(\varphi_{i+1,j} + \varphi_{i-1,j})}{2 + 2(1-\mu)K_{i,j} - \mu K_{i-1,j}} - \varphi_{i,j} \tag{10}$$

Then, the function updates the value in phi based on the SOR iteration formula:

$$\varphi_{i,j_{new}} = \varphi_{i,j} + sor * d\varphi \tag{11}$$

However, at the boundary conditions, there are points $\varphi_{i,j-1}$ outside the range, also known as ghost points. In this case, they could be represented by $\varphi_{i,j+1}$ as:

$$\varphi_{i,j-1} = \varphi_{i,j+1} - 2 \cdot h \cdot U\_\infty \cdot f'(x) \tag{12}$$

The residual at the current point (i, j), in this case, is:

$$d\varphi = \frac{\mu K_{i-1,j}(\varphi_{i-2,j} - 2\varphi_{i-1,j}) + 2\varphi_{i,j+1} - 2hU\_\infty \cdot f'(x) + (1-\mu)K_{i,j}(\varphi_{i+1,j} + \varphi_{i-1,j})}{2 + 2(1-\mu)K_{i,j} - \mu K_{i-1,j}} - \varphi_{i,j} \tag{13}$$

3.5. Main Function

The main function uses 32 grid points to discrete the domain and set the initial and boundary conditions. By iterating 1500 times, a convergent solution could be obtained with the error calculated every 100 iterations to ensure that the final error is less than e-7.

4. Results

By changing the value of β, the variations of the four Mach numbers within the specified spatial range were obtained. As shown in Figs. 3-5, it was found that when β=0.1, 0.15, and 0.175, the airflow remained in a continuous and stable state, but the rate of decrease in Mach number gradually decreased. When β=0.2 (Fig. 6), the variation of the Mach number was no longer regular, indicating that the airflow had become turbulent.

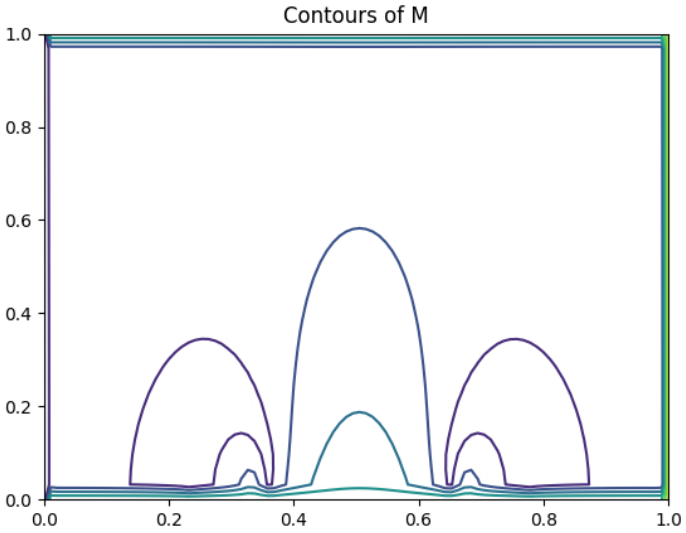

Figure 2. The contours of M when beta=0.1 (Photo/Picture credit: Original)

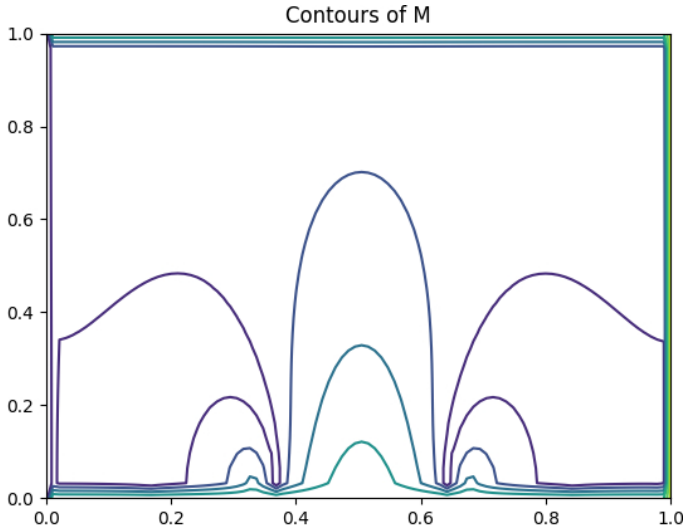

Figure 3. The contours of M when beta=0.15 (Photo/Picture credit: Original)

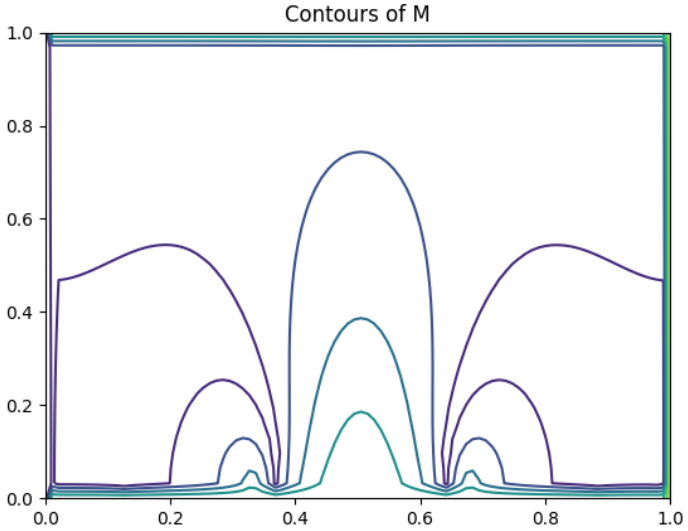

Figure 4. The contours of M when beta=0.175 (Photo/Picture credit: Original)

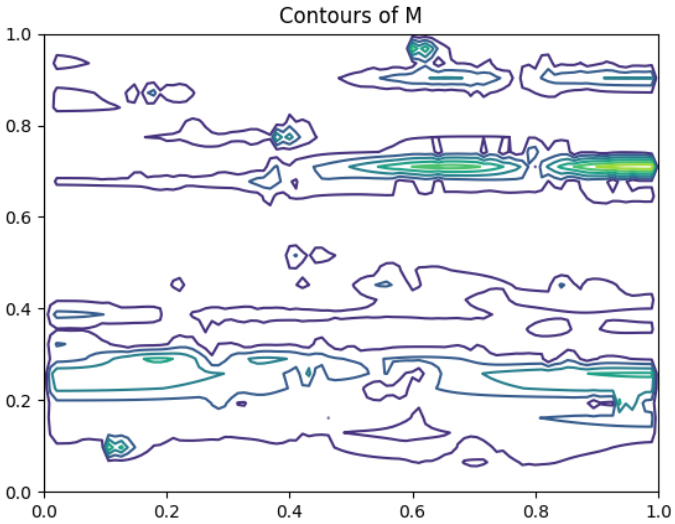

Figure 5. The contours of M when beta=0.2 (Photo/Picture credit: Original)

5. Conclusion

Due to the function $\beta \cdot \sin(\pi \cdot (x-1))$ being used to simulate the wing shape, where x represents the position on the wing, the shape of this function resembles a sine curve. Adjusting the value of β can change the difference between the peak and valley of the curve. The results above indicate that when the value of β is among 0.1, 0.15, and 0.175, the simulated wing shape of $\beta \cdot \sin(\pi \cdot (x-1))$ can generate relatively stable airflow. The stability of the airflow results in a relatively slow change in Mach number, meaning that the rate of decrease in Mach number gradually decreases. However, when the value of β increases to 0.2, the airflow becomes turbulent and cannot maintain a stable state. This leads to irregular changes in Mach number, potentially causing severe fluctuations and unpredictable variations, which may significantly impact aircraft flight safety.

The article employs a simplified two-dimensional Euler equation, neglecting complex fluid dynamic effects such as viscosity and turbulence. The method utilizes SOR iteration for the solution, which exhibits good convergence but requires a large number of iterations, resulting in low computational efficiency. Therefore, in the future, more sophisticated fluid dynamic models can be introduced to consider viscosity and turbulence effects to simulate wing shapes and airflow stability more accurately. Additionally, more efficient solution methods, such as multi-grid methods or parallel computing, can be explored to improve computational efficiency. Furthermore, other factors influencing airflow stability, such as wing geometry, airflow velocity, and temperature, can also be considered to further enhance simulation results and provide a more reliable basis for aircraft design and flight safety.

References

[1] Tian Yun, Gao Shiqi, Liu Peiqing, et al. Transonic buffet control research with two types of shock control bump based on RAE2822 airfoil. Chinese Journal of Aeronautics, 2017, 30 (5): 1681-1696.

[2] Rumeysa Şahin, Muammer Ayvazoğlu, et al. Effect of airfoil thickness on flow over the symmetric airfoils: part I-experimental analysis. In 2023 10th International Conference on Recent Advances in Air and Space Technologies (RAST), 2023, 01-06.

[3] Alison Zilstra, David A Johnson. Large eddy simulation of transitional separated flow over a low Reynolds number cambered airfoil. In ASME. Journal of Fluids Engineering, 2023.

[4] Liu Peiqing. Aerodynamic Characteristics of Supersonic Thin Airfoil and Wing. In Aerodynamics. Springer, Singapore, 2022. 715-767.

[5] Nirmith Kumar Mishra, Mohsin Naveed, et al. Characterization of supercritical airfoils using computational and experimental techniques. In AIP Conference Proceedings, 2023.

[6] Jing Shen. Analysis of current application of transonic flow aerodynamics. In Highlights in Science, Engineering and Technology, 2023.

[7] Tijdeman, Hendrik. Investigations of the transonic flow around oscillating airfoils. NLR-TR 77090 U, 1977.

[8] Raymer, Daniel. Aircraft design: a conceptual approach. American Institute of Aeronautics and Astronautics, 2012.

[9] Cheng, Fanrui, Yang Xu, Wenbo Zhou. Nozzle flow simulation by small disturbance approximation and Euler method. In Journal of Physics: Conference Series, 2021, 2012 (1): 012048.

[10] Ali, Kashif, et al. Application of the successive over relaxation method for analyzing the dusty flow over a surface subject to convective boundary condition. In Ain Shams Engineering Journal, 2023, 14 (8): 102044.